Nuclear Science and Techniques (2026) 37:95
https://doi.org/10.1007/s41365-026-01914-5

Plug-and-play digital twin based on multiscale multiphysics reduced-order method for simulation of nuclear reactor primary circuit

Ya-Hui Wang[1,2] · Ze-Long Zhao[1] · Hong-Hang Chi[1] · Zhe-Xian Liu[1] · Yu Ma[1,2]

Received: 7 June 2024 / Revised: 15 October 2024 / Accepted: 5 November 2024 / Published online: 21 March 2026

Abstract
Multiscale multiphysics simulation is a key technology for nuclear reactor system design and analysis. However, its application and development are limited by the complexity of cross-scale simulation coupling and long calculation times. To satisfy the real-time simulation requirements of modern reactor digital twins, this study establishes a digital twin of the reactor circuit using multiphysics and multiscale reduced-order methods. This digital twin is based on the plug-and-play approach, and all simulations of the components are replaced by independent 1D and 3D multiphysical reduced-order surrogate models. The complete system circuit can be composed of a combination of these surrogate models, which allows for the easy integration of new components and modification of existing components. A digital twin circuit is established for the test case. The reactor core is described using the 3D neutronics/thermal-hydraulics model, whereas the steam generator is described using the 3D CFD model. The other components, including the heat and cold pipes, are described using a 1D reduced-order model. The numerical results show that the digital twin can accurately predict the multiphysics and multiscale behavior of the reactor circuit. The maximum relative error of the tested circuit is not larger than 0.05%, and the simulation time can be reduced to less than 2 ms. The proposed plug-and-play digital twin can be used to develop a new real-time digital twin system that can support reactor system design and analysis.

Keywords Plug-and-play · Digital twin · Multiscale multiphysics · Reduced-order · Primary circuit

1 Introduction

The nuclear reactor system circuit contains a complicated intersection of multiphysics behaviors in which neutronics/thermal-hydraulics (NTH) processes are one of the main considerations in research and engineering [1]. Traditionally, a one-dimensional lumped parameter model has been used for multiphysics coupled calculations of reactor system circuits [2, 3]. Reactor core neutronics simulations often use a zero-dimensional (0D) point-kinetics (PK) model, whereas thermal-hydraulic behaviors are often approximated using a one-dimensional (1D) averaged model [4]. The reason for using these methods is that the three-dimensional (3D) simulation of the entire system circuit [5] requires excessive computational complexity. However, with the continuous improvement in the analysis requirements for advanced reactor systems and the development of computer technology, 0D and 1D system models fail to predict many local physical phenomena [6]. In addition, under certain special conditions, such as the accident state, the behavior of certain critical equipment must be analyzed in detail [7, 8].

To improve this condition, a compromise method, namely the multiscale method [9, 10], has been adopted by researchers, in which the main circuit is still simulated using 0D or 1D system codes, whereas the main

This work was supported by the Guangdong Basic and Applied Basic Research Foundation (No. 2025A1515011855), the Open Fund of State Key Laboratory of Nuclear Power Safety Technology and Equipment (No. SKL-2024-WT-05), and Sun Yat-sen University Key Cultivation Platform Project (No. 45000-12251016).

✉ Yu Ma
mayu9@mail.sysu.edu.cn

[1] Sino-French Institute of Nuclear Engineering and Technology, Sun Yat-sen University, Zhuhai 519082, China

[2] CNPRI-SYSU Joint Research Center of Coolant Chemistry for Nuclear Reactor, Zhuhai 519082, China

components, such as the reactor core and steam generator, are simulated using 3D multiphysics codes. The multiscale method shows better performance in obtaining a more comprehensive physical field distribution than the system method, while being much less computationally intensive than the fully 3D simulation of the entire system, which can significantly contribute to the improvement of the reactor design and the fulfillment of the continuously increasing reactor safety requirements [9]. Owing to these advantages, the multiscale method has attracted considerable attention from researchers and has been one of the main methods to study the safety and performance of reactor systems, which has promoted the development of multiple national projects, such as CASL [11], NURSIM, NURISP, and THINS [12]. Many researchers have also conducted extensive research on multiscale thermal-hydraulic coupling methods for nuclear reactor systems. Grunloh et al. [13] developed a multiscale flow analysis method for reactors by coupling CFD code STAR-CCM+ and the system thermal-hydraulic code TRACE and studied the domain overlap method for 1D and 3D computational data interaction. Through this coupling, neglected flow details in the system program calculations can be accurately captured. Cai et al. [14, 15] conducted a multiscale thermal-hydraulics analysis of the inherent safety of natural convection in the reactor core, combining 1D system code and 3D CFD simulation. The fluid flow and heat transfer of the fuel assembly were simulated using the 3D CFD method to analyze its flow features, for example, transverse mixing, which could not be described in the system codes, whereas the other components of the reactor circuit were simulated using 1D system codes. Aumille et al. [16] developed a 1D/3D coupled thermal-hydraulics code using the 1D system code ATHLET and 3D CFD code, and the results showed good agreement with ATHLET alone. Baviere et al. [17] coupled the 3D CFD code TRIO_U with the system thermal-hydraulics code CATHARE to analyze the thermal-hydraulic behavior of the natural circulation test of the French prototype sodium fast reactor (SFR) Phénix and obtained good agreement between the numerical and experimental data. Zou et al. [18] completed an ATHLET-OpenFOAM coupling code application and simulated an unprotected loss-of-flow accident process for a lead-cooled fast reactor. Zhao et al. [19] coupled the system code RELAP5 and 3D reactor core thermal-hydraulics code CTF to establish a novel multiscale method that can be applied to the coupling analysis of the pulsed reactor and can perform high-fidelity safety analyses of the pulsed reactor. Sanchez-Espinoza et al. [20] developed a series of multiscale thermal-hydraulics codes, in which the system calculation was imposed using the system code TRACE, whereas the 3D thermal-hydraulics behaviors were calculated using subchannel code suhChanFlow and the open-source CFD code trioCFD.

More recently, to consider the more accurate multiphysics and multiscale coupling behavior of reactor systems, coupled neutronics/thermal-hydraulics processes have been considered. Park et al. [21] conducted a multiscale analysis of the main steam management rupture accident in a nuclear power plant using 3D neutronics/thermal-hydraulic codes for reactor core analysis and 1D system analysis codes for other components. Luo et al. [7] developed a multiphysics multiscale code by combining the thermal-hydraulics code KMC-sub and the neutron diffusion code NDK using Fluent software. The shutdown operation of the reactor system was simulated, and the results showed good agreement with those of ATHLET. Lee et al. [22] combined the 1D system thermal-hydraulics code MRS covering most of the reactor coolant system, except the reactor pressure vessel, and used the 3D subchannel code CUPID-RV with three-dimensional neutron kinetics code MASTER for pressure water reactor analysis.

Thus, multiscale methods have received widespread attention and have made significant progress. However, although multiscale methods can better simulate complicated system behaviors, drawbacks such as long computation time and complex coupling calculations persist especially when using different calculation codes for coupling [23]. Typically, because of the differences in convergence, calculations at different scales often require different sweep formats, which makes coupling approaches between different scales more difficult [24]. In addition, because these multiscale models are designed for a specific system circuit, when the system design or operating conditions change, the numerical model must be modified, and the calculation should be restarted. Because of these limitations, achieving real-time or ultra-real-time predictions of digital twins remains challenging [25, 26]. The development of an efficient and flexible numerical method is still required to satisfy the needs of advanced reactor digital twins. For this phenomenon, using a surrogate model [27–29] that directly obtains the physical quantity of the outlet from the inlet conditions without considering the numerical stability of the sweep process may be a good alternative.

To establish a simple and efficient surrogate model, the reduced-order method [30] can be an effective, cheap, and accurate method that replaces the original calculation model (denoted as the full-order model, FOM) with a reduced-order model (ROM) under a significantly reduced dimensionality and a controlled loss of accuracy to ensure the reliable evaluation of the reduced model at a substantially reduced computational cost [31]. The implementation of the ROM can be divided into two stages: offline and online. In the offline stage, FOM calculations are used to obtain snapshots, that is, the distributions of the physical quantities of concern

under different states. The ROM bases are then constructed by performing modal decomposition on the snapshots, such as the proper orthogonal decomposition (POD) method. During the online stage, numerical techniques, such as data interpolation and least-squares regression, were employed to compute the POD basis coefficients for the predicted conditions. The physical quantity distributions for these predicted conditions were reconstructed by linearly combining the POD basis functions with the POD coefficients. In recent years, the ROM has been widely used in various fields such as fluid flow [32, 33], electrical kinetics [34], vibro-acoustic simulation [35], and CO_2 capture [36].

In nuclear engineering, the ROM has also been widely used in neutronics and thermal-hydraulic predictions [37–40]. In neutronics calculations, the ROM has been used for neutron transport and depletion dynamics calculations. German et al. [41] and Dominesey et al. [39] extended ROM to neutron diffusion and transport eigenvalue calculations. Roberts et al. [42] applied a ROM based on dynamic mode decomposition to accelerate the power iteration of the neutron diffusion eigenvalue calculation. Chen et al. [43] applied a nonintrusive ROM to accelerate neutron diffusion calculations in an IAEA 3D reactor core. Chi et al. [44] and Wang et al. [45] developed a neutron transport ROM in both detailed and nodal calculations and extended the detailed neutron transport ROM to neutron transport kinetics calculations [46]. Gong et al. [38] developed a reduced-order method based on the dynamic mode decomposition for xenon dynamic forecasting. Based on the application of the ROM in neutronics prediction, Argaud et al. [47] applied the ROM to optimize the sensor placement in nuclear reactors. In thermal-hydraulics calculations, Alsayyari et al. [48] and German et al. [49] extended the ROM for multiphysics calculations in a molten salt fast reactor and analyzed the influence of the molten salt flow on the power distribution. Kang et al. [50] constructed a ROM based on POD and machine learning to predict the thermal-hydraulic behavior in the subchannels of fuel assemblies in nuclear reactor cores. Lorenzo et al. [51] developed an ROM for Navier–Stokes equations and thermal-hydraulic problems based on the finite volume method and POD. The model was numerically validated using a homogeneous lid-driven cavity reactor model that accurately reproduced the temperature and velocity fields. Star et al. [52] developed a ROM based on RELAP5 and OpenFOAM coupling and showed good accuracy. Manthey et al. [53] developed a two-phase flow ROM by combining the system program codes ATHLET and POD. This ROM demonstrated good numerical calculation accuracy for the simulation of two-phase flows in natural convection or high-pressure environments. Using these techniques, the calculation time for complex physical processes can be reduced to milliseconds [54, 55], which is expected to achieve real-time or even ultra-real-time digital twins in nuclear reactor systems. However, the studies on neutron transport and thermal hydraulics have been relatively independent. Multiphysics and multiscale applications require further development.

From this perspective, the proposed work establishes a plug-and-play digital twin based on a multiscale multiphysics reduced-order method for nuclear reactor circuit systems. The 1D system thermal-hydraulics reduced-order surrogate model was established for the main circuit. The 3D CFD thermal-hydraulics reduced-order surrogate model was established for the steam generator, and a 3D neutronics/thermal-hydraulics reduced-order surrogate model was established for the reactor core. By concatenating the reduced-order surrogate models of all components, a ROM-based multiphysics digital twin for the nuclear reactor circuit system was established. The remainder of this paper is organized as follows: in Sect. 2, the mathematical theories of this work are described, including the full-order model, reduced-order surrogate model, and digital twin circuit; in Sect. 3, the digital twin circuit is verified by testing a typical circuit system; and Sect. 4 provides some of the main conclusions of this work.

2 Mathematical theory

2.1 Multiscale coupled simulation of primary circuit

The multiscale coupled simulation of the primary circuit consists of two parts: a one-dimensional (1D) system calculation for the auxiliary components of the primary circuit and a three-dimensional (3D) calculation of the critical equipment. 3D computing is used to study the detailed behavior of key equipment in nuclear power systems, such as the performance testing of newly developed equipment and performance analyses of key equipment under certain operating conditions. In this work, the reactor core and steam generator (SG) are simulated in 3D as the key components, whereas the other components were simulated using a one-dimensional system model. In the following section, the mathematical theories of the multiscale calculations are described in detail.

2.1.1 Three-dimensional neutronics/thermal-hydraulics model of reactor core

The reactor core is a key component of a nuclear reactor system, and studying its internal neutronic/thermal-hydraulic behavior is crucial for analyzing the safety and performance of the core. Therefore, the 3D coupled neutronics/thermal-hydraulics behavior was considered for analyzing the reactor core.

The steady-state multigroup neutron diffusion equation was used to describe the neutronic behavior within the reactor core.

$$
\begin{aligned}
&-\nabla\cdot(D_g\nabla\phi_g)+\Sigma_{\mathrm{r},g}\\
&=\sum_{g'\neq g}^{G}\Sigma_{\mathrm{s},g'-g}\phi_{g'}+\frac{\chi_g}{k_{\mathrm{eff}}}\sum_{g'=1}^{G}\nu\Sigma_{\mathrm{f},g'}\phi_{g'},
\end{aligned}
\tag{1}
$$

where ϕ_g represents the neutron flux corresponding to g-th energy group, $g = 1, ..., G$; here, we omitted the independent variable spatial vector $\boldsymbol{r}$, D_g, $\Sigma_{\mathrm{r},g}$, $\nu\Sigma_{\mathrm{f},g}$ are the neutron diffusion coefficient, macroscopic removal cross section, and macroscopic neutron production $\Sigma_{\mathrm{s},g'-g}$ represents the macroscopic scattering cross section from group g' to group g. χ_g is the neutron fission spectrum, and k_{eff} is the effective multiplication factor. When considering the neutronic/thermal-hydraulic coupling, the diffusion coefficient and cross sections can be rewritten as the functions of temperature: $D = D(T_{\mathrm{u}}, T_{\mathrm{m}}, D_{\mathrm{m}})$ and $\Sigma_{\mathrm{x}} = \Sigma_{\mathrm{x}}(T_{\mathrm{u}}, T_{\mathrm{m}}, D_{\mathrm{m}})$, where T_{u} and T_{m} are the fuel temperature and moderator temperature, respectively; D_{m} is the moderator density. Because of the enormous computational effort required for full-core detailed neutron diffusion simulations and because the average power and temperature distribution of pin cells or assemblies are usually sufficient for engineering purposes, this study employs the nodal method [56] to solve the reactor core neutron diffusion equation. For the steady-state thermal-hydraulic calculations, the single-channel method [57, 58] was used for each moderator channel. The hydraulic calculation of each channel was achieved based on the one-dimensional mass, momentum, and energy conservation as follows:

$$
\begin{aligned}
&\frac{\partial G_{\mathrm{m}}}{\partial z}=0,\\
&\frac{\partial}{\partial z}\left(\frac{G_{\mathrm{m}}^2}{\rho_{\mathrm{m}}}\right)=-\frac{\partial p_{\mathrm{c}}}{\partial z}-\frac{fG_{\mathrm{m}}|G_{\mathrm{m}}|}{2D_{\mathrm{e}}\rho_{\mathrm{m}}}-\rho_{\mathrm{m}}g\cos(\theta),\\
&G_{\mathrm{m}}\frac{\partial H_{\mathrm{m}}}{\partial z}=\frac{q_{\mathrm{l}}P_{\mathrm{h}}}{A_{\mathrm{z}}}+\frac{G_{\mathrm{m}}}{\rho_{\mathrm{m}}}\left(\frac{fG_{\mathrm{m}}|G_{\mathrm{m}}|}{2D_{\mathrm{e}}\rho_{\mathrm{m}}}+\frac{\partial p_{\mathrm{c}}}{\partial z}\right),
\end{aligned}
\tag{2}
$$

where G_{m}, f, g, ρ_{m}, H_{m}, p_{c}, D_{e}, A_{z}, P_{h} are coolant mass flux, channel friction factor, gravitational acceleration, coolant enthalpy, core pressure, flow channel equivalent diameter, flow channel area, and heated perimeter, respectively; θ is flow channel inclination angle; q_{l} is fuel rod line power density, which is calculated as:

$$
q_{\mathrm{l}}=\int_{A_{\mathrm{u}}}q_{\mathrm{v}}\mathrm{d}A\int_{A_{\mathrm{u}}}F_{\mathrm{u}}E_{\mathrm{f}}\sum_{g'=1}^{G}\Sigma_{\mathrm{f},g'}\phi_{g'}\mathrm{d}A,
\tag{3}
$$

where q_{v} is the volume power density; F_{u} is the proportion of heat released from the pellets to the total heat release, which is generally taken as 97.4% in engineering; E_{f} is the energy released from a single fission; and A_{u} is the cross-sectional area of the fuel pellets. Under the single-phase assumption, the pressure drop and fluid enthalpies of the reactor were calculated by considering the inlet temperature, inlet pressure, and inlet mass flux. After the enthalpy and pressure were calculated, the temperature and density distributions along the channel were obtained using the IF97 thermophysical properties table [59].

The thermal calculations mainly involve the radial one-dimensional thermal conductivity calculation of the fuel rod, including the fuel pellet, gap, and cladding. A fuel pellet can be described as:

$$
\frac{1}{r}\frac{\mathrm{d}}{\mathrm{d}r}\left(\kappa_{\mathrm{u}}r\frac{\mathrm{d}T_{\mathrm{u}}}{\mathrm{d}r}\right)+q_{\mathrm{v}}=0,
\tag{4}
$$

where r represents the position of the radial coordinates, T_{u} and κ_{u} are the temperature and heat conductivity of the fuel pellet, respectively, and for the gap and cladding, this equation is generally rewritten as

$$
\frac{1}{r}\frac{\mathrm{d}}{\mathrm{d}r}\left(\kappa_{\mathrm{g}}r\frac{\mathrm{d}T_{\mathrm{g}}}{\mathrm{d}r}\right)=0,
\tag{5}
$$

where T_{g} and κ_{g} denote the general temperature and heat conductivity of the gap and cladding, respectively.

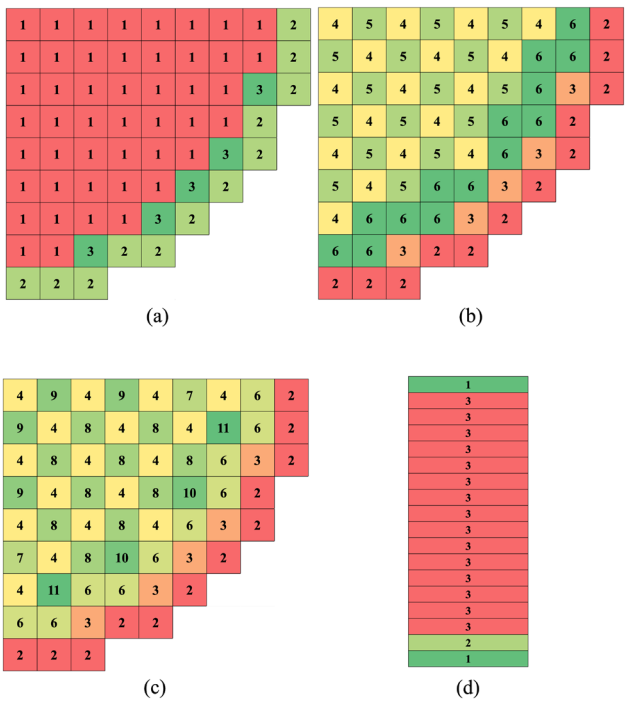

Fig. 1 (Color online) Geometry of NEACRP reactor [60], including (a) layer 1, (b) layer 2, (c) layer 3, and (d) axial distribution

This is the coupled neutronics/thermal-hydraulics model that is used in this study. As an example, a 3D NEA-CRP reactor core was used in this study, whose design references the literature [60], as shown in Fig. 1. The neutronic behavior of the reactor core was simulated using the open-source software ADPRES [60]. The 3D thermal-hydraulic process was calculated using our self-developed code, which was coupled with ADPRES for neutronics/thermal-hydraulics coupling. In the calculation, vacuum and reflective boundaries were used for the core boundary and internal symmetry plane in neutron diffusion, respectively. The inlet temperature, inlet pressure, and inlet mass flux were provided for the thermal-hydraulic calculation. In the radial direction, each assembly was divided into two ×2 nodals, and the axial direction was divided into 18 layers. The thermal-hydraulic and physical calculations used a similar mesh configuration.

2.1.2 Three-dimensional CFD calculation of steam generator

Another carefully considered component is the steam generator (SG), which is an important component of a nuclear reactor's primary circuit and must always be optimized for design. To this end, this study used the three-dimensional CFD method to analyze the detailed thermal-hydraulic behavior inside the steam generator. A schematic of the steam generator is shown in Fig. 2, in which the red and blue parts represent the primary and secondary sides, respectively. To reduce computational cost, an equivalent U-tube model was used instead of a complete steam generator [61], as shown in Fig. 3. In this simulation, the governing equations for the primary side are expressed as follows:

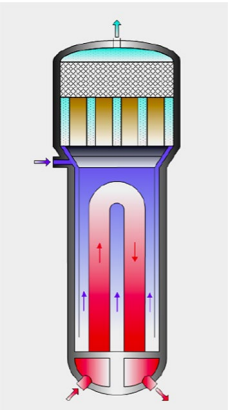

Fig. 2 (Color online) Schematic of steam generator (red and blue represent the primary and secondary sides, respectively)

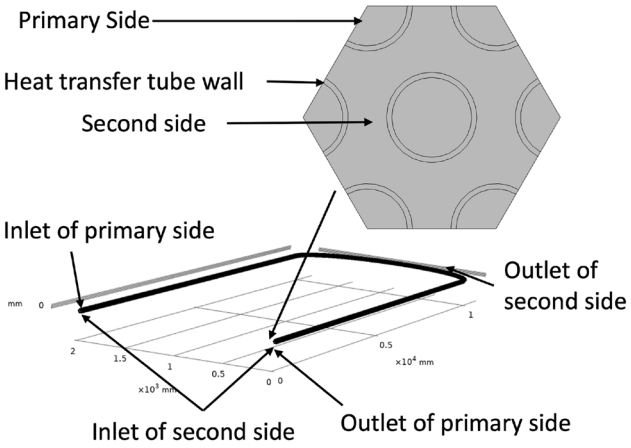

Fig. 3 Schematic of equivalently SG model

$$
\begin{aligned}
&\nabla \cdot (\rho \boldsymbol{u}) = 0\\
&\rho(\boldsymbol{u} \cdot \nabla)\boldsymbol{u} = \nabla \cdot (p\boldsymbol{I} + \boldsymbol{K}) + \boldsymbol{F}\\
&\rho(\boldsymbol{u} \cdot \nabla)k = \nabla \cdot \left[\left(\mu + \frac{\mu_{\mathrm{t}}}{\sigma_{\mathrm{k}}}\right)\nabla k\right] + P_{\mathrm{k}} - \rho\varepsilon\\
&\rho(\boldsymbol{u} \cdot \nabla)\varepsilon = \nabla \cdot \left[\left(\mu + \frac{\mu_{\mathrm{t}}}{\sigma_{\varepsilon}}\right)\nabla \varepsilon\right] + C_{\varepsilon 1}\frac{\varepsilon}{k}P_{\mathrm{k}} - C_{\varepsilon 2}\rho\frac{\varepsilon^2}{k}\\
&\rho C_{\mathrm{p}}\boldsymbol{u} \cdot \nabla T - \nabla \cdot (\kappa \nabla T) = Q\\
&\boldsymbol{K} = (\mu + \mu_{\mathrm{t}})\left(\nabla \boldsymbol{u} + (\nabla \boldsymbol{u})^{\mathrm{T}}\right)\\
&\qquad - \frac{2}{3}(\mu + \mu_{\mathrm{t}})(\nabla \cdot \boldsymbol{u})\boldsymbol{I} - \frac{2}{3}\rho k\boldsymbol{I}\\
&\mu_{\mathrm{T}} = \rho C_{\mu}\frac{k^2}{\varepsilon}\\
&P_{\mathrm{k}} = \mu_{\mathrm{T}}\left(\nabla \boldsymbol{u} : (\nabla \boldsymbol{u} + (\nabla \boldsymbol{u})^{\mathrm{T}}) - \frac{2}{3}(\nabla \cdot \boldsymbol{u})^2\right) - \frac{2}{3}\rho k \nabla \cdot \boldsymbol{u},
\end{aligned}
\tag{6}
$$

where ρ_{p}, $\mathbf{u}$, p, k, ε, T, C_{p}, μ, μ_{t}, and κ are density, velocity, pressure, turbulent kinetic energy, turbulent dissipation rate, temperature, specific heat, viscosity, turbulent viscosity, and thermal conductivity, respectively; Q is heat source; $\boldsymbol{F}$ is the fluid force term; $C_{\varepsilon 1} = 1.44$, $C_{\varepsilon 2} = 1.92$, $C_{\mu} = 0.09$, $\sigma_{\mathrm{k}} = 1.0$ and $\sigma_{\varepsilon} = 1.3$ are model constants. Neglecting the stress, strain, and movement of the heat transfer tubes, the governing equation of the heat transfer tube wall can be expressed as

$$
\nabla \cdot \left(\frac{\kappa_{\mathrm{w}}}{c_{\mathrm{pw}}}\nabla T_{\mathrm{w}}\right), \tag{7}
$$

where κ_{w}, c_{pw}, and T_{w} denote the thermal conductivity, specific heat capacity, and temperature of the heat transfer tube wall, respectively.

For the secondary side, refer to Sun et al. [62]. The liquid is solved as a continuous phase (denoted by l), whereas the vapor is solved as the dispersed phase (denoted by v).

The ensemble-averaged conservation equations in the two-fluid model for each phase can be written as

$$\begin{aligned}
&\nabla \cdot (\alpha_i \rho_i \boldsymbol{u}_i) = \dot{m}_{i,j} \\
&\nabla \cdot (\alpha_i (\rho_i \boldsymbol{u}_i \boldsymbol{u}_i - \mu_i^{\mathrm{eff}} (\nabla \boldsymbol{u}_i + (\nabla \boldsymbol{u}_i)^{\mathrm{T}}))) \\
&= \alpha_i (\rho_i g - \nabla p_i) + \boldsymbol{F}_{i,j} + \dot{m}_{i,j} \boldsymbol{u}_i \\
&\nabla \cdot (\alpha_i (\rho_i \boldsymbol{U}_i H_i - \lambda_i \nabla T_i)) = Q_{i,j}
\end{aligned}, \tag{8}$$

where $i,j = \{\mathrm{l,v}\}$ for the liquid and vapor phases, α_i, ρ_i, $\boldsymbol{u}_i$, p_i, μ_i^{eff}, λ_i, and T_i are the volume fraction, density, velocity, pressure, effective dynamic viscosity, thermal conductivity, and temperature of i-th phase, respectively. $\dot{m}_{i,j}$ represents the mass transfer rate from phase i to j, $\boldsymbol{F}_{i,j}$ represents the force acting on phase i relative to phase j, $Q_{i,j}$ represents the total heat transfer from phase i to j.

On the secondary side, the vapor phase is regarded as a laminar flow and the liquid phase is described using the $k-\varepsilon$ turbulence model:

$$\begin{aligned}
&\nabla \cdot \left(\rho_{\mathrm{l}} k_{\mathrm{l}} \boldsymbol{u}_{\mathrm{l}}\right) = \nabla \cdot \left[\left(\mu_{\mathrm{tl}} + \frac{\mu_{\mathrm{tl}}}{\sigma_{\mathrm{k}}}\right) \nabla \cdot k_{\mathrm{l}}\right] + P_{\mathrm{kl}} - \rho_{\mathrm{l}} \varepsilon_{\mathrm{l}} \\
&\nabla \cdot \left(\rho_{\mathrm{l}} \varepsilon_{\mathrm{l}} \boldsymbol{u}_{\mathrm{l}}\right) \\
&= \nabla \cdot \left[\left(\mu_{\mathrm{tl}} + \frac{\mu_{\mathrm{tl}}}{\sigma_{\varepsilon}}\right) \nabla \cdot \varepsilon_{\mathrm{l}}\right] + \frac{C_{1\varepsilon}}{k_{\mathrm{l}}} P_{\mathrm{kl}} - C_{2\varepsilon} \rho_{\mathrm{l}} \frac{\varepsilon_{\mathrm{l}}^2}{k_{\mathrm{l}}} \\
&P_{\mathrm{kl}} = \mu_{\mathrm{l}}^{\mathrm{eff}} \nabla \boldsymbol{u} \cdot \left[\nabla \boldsymbol{u} + (\nabla \boldsymbol{u})^{\mathrm{T}}\right] \\
&\mu_{\mathrm{tl}} = C_{\mu} \rho_{\mathrm{l}} \frac{k_{\mathrm{l}}^2}{\varepsilon_{\mathrm{l}}} \\
&\mu_{\mathrm{l}}^{\mathrm{eff}} = C_{\mu} \rho_{\mathrm{l}} \frac{k_{\mathrm{l}}^2}{\varepsilon_{\mathrm{l}}} + C_{\mu \mathrm{b}} d_{\mathrm{b}} \alpha_{\mathrm{l}} \left|\boldsymbol{u}_{\mathrm{v}} - \boldsymbol{u}_{\mathrm{l}}\right|
\end{aligned} \tag{9}$$

where d_{b} represents the bubble detachment diameter, $C_{\mu \mathrm{b}} = 0.6$ is a constant. All the other variables follow the same definitions as those in Eq. (6). The heated boiling process on the secondary side was simulated using a thermal phase transition model that considers the mass, momentum, and energy transfer across the interfaces between the two phases. The details of these models can be found in Refs. [62, 63].

In this study, the detailed thermal-hydraulic behavior within SG was calculated using the finite-element method (FEM) with the COMSOL software [64]. Figure 4 illustrates the mesh configuration of SG. After grid-independent verification, 1478800 meshes were used for the calculation. To calculate the stability, the inlet boundaries were applied to the temperature and velocity distributions, whereas the outlet boundary was applied to the pressure distribution.

The detailed CFD model used for the steam described above. For further applications, further research can be conducted, such as full-geometry and porous-medium approaches [65].

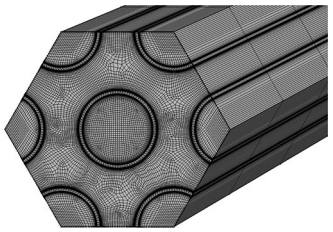

Fig. 4 Mesh configuration of equivalently SG model

2.1.3 System model

Other components, including the pipelines, pressurizer, and main pump, were simulated using system models. Because the detailed temperature and pressure distributions inside the pipeline are not as important for the entire core system circuit, a one-dimensional thermal-hydraulics model is used for the pipelines:

$$\frac{\mathrm{d}\left(\rho_{\mathrm{p}} u_{\mathrm{p}}\right)}{\mathrm{d}x} = 0, \tag{10}$$

$$\frac{\mathrm{d}\left(\rho_{\mathrm{p}} u_{\mathrm{p}} u_{\mathrm{p}}\right)}{\mathrm{d}x} = \frac{\mathrm{d}}{\mathrm{d}x}\left(\mu_{\mathrm{p}} \frac{\mathrm{d}u_{\mathrm{p}}}{\mathrm{d}x}\right) - \frac{\mathrm{d}P_{\mathrm{p}}}{\mathrm{d}x} - \frac{1}{2} \frac{f_{\mathrm{p}}}{d} \rho {u_{\mathrm{p}}}^2 - \rho_{\mathrm{p}} g \sin \theta_{\mathrm{p}}, \tag{11}$$

where the subscript p indicates the physical quantity of the pipeline, θ represents the pipe tilt angle, and d represents the pipe inner diameter (m); f_{p} represents the Darcy friction factor in the pipes, which can be expressed as follows [66]:

$$\begin{cases} f_{\mathrm{p}} & = \frac{64}{Re}, Re_{\mathrm{D}} \le Re_{\mathrm{c}} \\ \frac{1}{{f_{\mathrm{p}}}^{1/2}} & = -2 \log\left(\frac{\varepsilon_{\mathrm{p}}/d}{3.7} + \frac{2.51}{Re_{\mathrm{D}} {f_{\mathrm{p}}}^{1/2}}\right), Re_{\mathrm{D}} > Re_{\mathrm{c}} \end{cases} \tag{12}$$

where Re_{D} is the pipe Reynolds number, Re_{c} is the critical Reynolds number, and ε_{p} is the pipe roughness (m).

In the discrete heat transfer pipe model, an energy equation must be incorporated into the continuity and momentum equations. The energy equations can be expressed as

$$\frac{\mathrm{d}\left(\rho_{\mathrm{p}} u_{\mathrm{p}} h_{\mathrm{p}}\right)}{\mathrm{d}x} - \frac{\mathrm{d}}{\mathrm{d}x}\left(\kappa_{\mathrm{p}} \frac{\mathrm{d}T_{\mathrm{p}}}{\mathrm{d}x}\right) = q_{\mathrm{p}}, \tag{13}$$

where q_{p} denotes the volumetric heat loss ($\mathrm{W/m^3}$). Using the above equations, the thermal-hydraulic process within different types of pipelines can be simulated, and each pipe is divided into 100 grids for calculation. The pressurizer is taken as a pressure containment boundary of the primary circuit, through which the circuit pressure will be adjusted to the set pressure, such as 15.5 MPa [67]. The effect of the main pump is reflected in the change in pressure (head) in the primary circuit, and its model relationship can be

obtained from the head characteristic curve [68]. Therefore, in this system model, these two components are approximated using zero-dimensional (0D) models.

2.1.4 Multiscale multiphysics primary circuit model

The multiscale multiphysics primary circuit system investigated in this study is illustrated in Fig. 5, which includes the 3D reactor, 3D steam generator, 1D pipelines, 0D pressurizer, and main pump. For plug-and-play, all components were calculated using independent codes. In this study, these calculations are referred to as the full-order model (FOM).

Normally, this multiscale model can be established by coupling the above component models with inlet and outlet values. The calculation is implemented by sequentially solving the models of each component, transferring their output values to the input values of the downstream components, and iterating until the loop converges. Through these coupling processes, the primary circuit system is simulated in a multiscale manner, and the behavior of the entire system is obtained by aggregating the behavior of its individual components. However, the necessity for coupling and transferring data across various software platforms presents significant challenges. These challenges are compounded by the substantial computational time required for integrated simulations. In addition, different methods for solving different components cause greater difficulties in this coupling. As mentioned earlier, in solving the steam generator using the CFD method, to calculate the stability, the inlet boundaries are applied to the temperature and velocity distributions, while the outlet boundary is applied to the pressure distribution. Under these conditions, the classical forward sweep method is not applicable because the upstream pressure is unknown, whereas the downstream pressure is known. To ensure the computational stability of the circuit model, a forward sweep–backward sweep method is proposed, in which the velocity and temperature can be calculated using the forward sweep method (e.g., clockwise), whereas the pressure should be calculated using the backward sweep method (e.g., counterclockwise). Because of this requirement, existing system programs must be significantly modified, and the universality of the programs will be reduced. For this phenomenon, a surrogate model that directly obtains the outlet physical quantity from the inlet conditions without considering the numerical stability of the sweep process may be a good alternative. The inlet pressure of the steam generator can be obtained by setting different outlet pressures and establishing a mapping relationship. To this end, the reduced-order method (ROM) is effective for constructing surrogate models.

In the following section, we present a plug-and-play multiscale reduced-order model for the primary circuit system, in which surrogate models for all components are established and connected. The external file coupling and integration processes in multiscale coupling calculations can be eliminated.

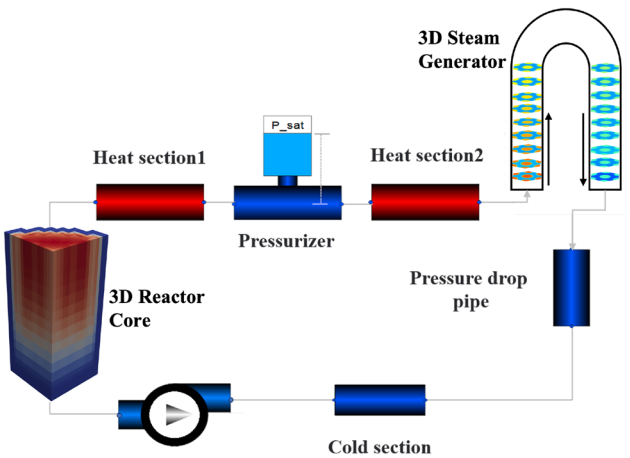

Fig. 5 (Color online) Schematic of equivalently SG model

2.2 Digital twin based on multiscale multiphysics ROM for primary circuit

Predictions of the diverse behaviors of reactor systems require a reduced-order model for a full system circuit that possesses adequate generalization capabilities. Typically, generating such a reduced-order model requires a large number of circuit snapshots, which can be readily achievable in one-dimensional system simulations. However, in multiscale simulations, this requirement becomes particularly challenging owing to the complexity of the implementation and large computing costs.

Nevertheless, adopting a divide-and-conquer strategy is a promising solution. The behavior of a system is an aggregation of the behaviors of its individual components. The complex behavior of the entire system can be described by considering the behavior coupling of various components under a range of state parameters, e.g., inlet conditions, the complex behavior of the entire system can be described. Therefore, a digital twin for the entire circuit can be constructed by developing separate reduced-order surrogate models for each component and subsequently integrating them to form a system circuit. This approach obviates the need for extensive system circuit snapshots as well as allows various simulation software to operate independently, thereby eliminating the need for direct application coupling. Furthermore, this methodology facilitates the establishment of different types of circuits by replacing the corresponding components, similar to a plug-and-play system.

2.2.1 Creation of snapshots

Snapshots of each component were obtained by conducting system or 3D calculations within the corresponding component state parameter ranges. For each component, we used the inlet or outlet parameters as the state parameters according to the requirements of the independent component calculation. For the reactor core, the core power P_{n}, inlet mass flux G_{in}, inlet temperature T_{in}, and inlet pressure p_{in} are considered as its state parameters, which can be written as $\boldsymbol{\mu}_{\mathrm{c}} = \{T_{\mathrm{in}}, G_{\mathrm{in}}, p_{\mathrm{in}}, P_{\mathrm{n}}\}$. For pipelines, the inlet velocity U_{in}, inlet temperature T_{in}, and inlet pressure p_{in} are considered as their state parameters, which can be written as $\boldsymbol{\mu}_{\mathrm{p}} = \{T_{\mathrm{in}}, U_{\mathrm{in}}, p_{\mathrm{in}}\}$. The above state parameters are consistent in both the snapshot calculations and reduced-order circuit calculations.

Specifically, for the steam generator, two types of state parameters are used. Because the primary and secondary circuits are strongly coupled under normal operating conditions, each set of SG primary circuit state parameters corresponds to a specific secondary circuit state. If the primary circuit state parameters are specified, the secondary circuit state can be uniquely determined. Therefore, only the primary loop-state parameters must be specified under normal operating conditions. For snapshot calculation, the inlet temperature T_{in}, velocity U_{in} and outlet pressure p_{out} are considered for computing stability [61], which can be written as $\hat{\boldsymbol{\mu}}_{\mathrm{s}} = \{T_{\mathrm{in}}, U_{\mathrm{in}}, p_{\mathrm{out}}\}$. For reduced-order calculation in circuit coupling, to achieve sequential connection of different components between circuits, the inlet parameters are still used as the state parameters of the reduced-order surrogate model, namely $\boldsymbol{\mu}_{\mathrm{s}} = \{T_{\mathrm{in}}, U_{\mathrm{in}}, p_{\mathrm{in}}\}$. Because of the absence of a CFD calculation process in the reduced-order surrogate model, no stability issue is detected with this state parameter setting.

After defining the state parameters of each component, the ranges of state parameters for each component to calculate snapshots should be determined. This was achieved by conducting one-dimensional system calculations on typical circuits under different core power conditions and summarizing the inlet and outlet parameter ranges of each component.

2.2.2 Calculation of reduced bases

One of the main processes of the reduced-order surrogate model is to extract reduced bases from snapshots. In this study, the proper orthogonal decomposition (POD) method was used because of its maturity and reliability. For self-consistency, the basic properties of the POD were introduced. Taking the reactor core as an example, we consider a collection of N temperature and power snapshots $\boldsymbol{A}_{\mathrm{T}} = \{\boldsymbol{u}_{\mathrm{T}}(\boldsymbol{\mu}_k)\}_{k=1}^{N}$ $\boldsymbol{A}_{\mathrm{P}} = \{\boldsymbol{u}_{\mathrm{P}}(\boldsymbol{\mu}_k)\}_{k=1}^{N}$ corresponding to the discrete parameter set $D = \{\boldsymbol{\mu}_1, ..., \boldsymbol{\mu}_N\}$ for power and temperature distributions. The snapshot for k-th parameter $\boldsymbol{\mu}_k$ is defined as:

$$\begin{aligned} \boldsymbol{u}_{\mathrm{P}}(\boldsymbol{\mu}_k) &= (P_1, ..., P_i, ..., P_M)_k^{\mathrm{T}}, \\ \boldsymbol{u}_{\mathrm{T}}(\boldsymbol{\mu}_k) &= (T_1, ..., T_i, ..., T_M)_k^{\mathrm{T}}, \end{aligned} \tag{14}$$

where $\boldsymbol{u}_{\mathrm{P}}(\boldsymbol{\mu}_k)$ and $\boldsymbol{u}_{\mathrm{T}}(\boldsymbol{\mu}_k)$ represent the power and temperature distributions within the reactor core corresponding to k-th state parameter combination $\boldsymbol{\mu}_k$, respectively; M is the total mesh number, the subscript i indicates the mesh index, T_i and P_i are the coolant temperature and power distribution corresponding to i-th mesh node, respectively. The correlation matrix $\boldsymbol{S}$ is then formed by computing the inner product of each pair of snapshots as follows:

$$\boldsymbol{S}_\alpha = \boldsymbol{A}_\alpha^{\mathrm{T}} \boldsymbol{A}_\alpha, \quad \alpha = P, T. \tag{15}$$

The set of eigenvalues $\{\lambda_{\alpha,i}\}_{i=1}^{N}$ and the corresponding eigenvector $\{\boldsymbol{X}_{\alpha,i}\}_{i=1}^{N}$ of the matrix $\boldsymbol{S}_\alpha$ are computed to obtain the POD bases. The set of POD bases $\{\boldsymbol{P}_{\alpha,i}\}_{i=1}^{N}$ can be determined according to

$$\boldsymbol{P}_{\alpha,i} = \frac{1}{\sqrt{\lambda_{\alpha,i}}} \boldsymbol{A}_\alpha \boldsymbol{X}_{\alpha,i}, \quad \alpha = P, T, \quad i = 1, 2, ..., N \tag{16}$$

where $\boldsymbol{P}_{\alpha,i}$ is ith-order POD basis vector of the αth variable. The magnitude of i-th eigenvalue $\lambda_{\alpha,i}$ describes the relative importance of the i-th order POD basis vector $\boldsymbol{P}_{\alpha,i}$. The first N_{p} orders of the POD bases are used to establish the reduced-order model, which is defined by the following regulation:

$$\begin{aligned} N_{\mathrm{p}} &= \arg\min\{R_\alpha(N_{\mathrm{p}}) : R_\alpha(N_{\mathrm{p}}) < \epsilon\} \\ R_\alpha(N_{\mathrm{p}}) &= 1 - \sum_{i}^{N_{\mathrm{p}}} \lambda_{\alpha,i} / \sum_{i}^{N} \lambda_{\alpha,i} \end{aligned} \quad , \quad \alpha = P, T, \tag{17}$$

where ϵ is set to 10^{-8} to ensure efficient information. Using this approach, the collection of POD bases is defined as $\{\boldsymbol{P}_{\alpha,i}\}_{i=1}^{N_{\mathrm{p}}}$. The snapshots can be expressed using a linear combination of POD bases as follows:

$$\begin{aligned} \boldsymbol{u}_T(\boldsymbol{\mu}_k) &= \sum_{i=1}^{N_{\mathrm{p}}} c_{T,i}(\boldsymbol{\mu}_k) \boldsymbol{P}_{T,i}, \\ \boldsymbol{u}_P(\boldsymbol{\mu}_k) &= \sum_{i=1}^{N_{\mathrm{p}}} c_{P,i}(\boldsymbol{\mu}_k) \boldsymbol{P}_{P,i}, \end{aligned} \tag{18}$$

where $c_{T,i}(\boldsymbol{\mu}_k)$ and $c_{P,i}(\boldsymbol{\mu}_k)$ are i-th basis coefficients of the temperature and power distributions corresponding to $\boldsymbol{\mu}_k$.

These were the reduced bases calculated for the reactor cores. Using a similar approach, the reduced bases for other components can be obtained. In contrast, for the steam generator, the velocity and temperature were used as snapshots:

$$\begin{aligned}\boldsymbol{u}_T(\boldsymbol{\mu}_k) &= (T_1, ..., T_M)_k^{\mathrm{T}},\\ \boldsymbol{u}_u(\boldsymbol{\mu}_k) &= (u_1, ..., u_M)_k^{\mathrm{T}},\\ \boldsymbol{u}_v(\boldsymbol{\mu}_k) &= (v_1, ..., v_m)_k^{\mathrm{T}},\\ \boldsymbol{u}_w(\boldsymbol{\mu}_k) &= (w_1, ..., w_m)_k^{\mathrm{T}},\end{aligned} \tag{19}$$

where u, v and w denote the velocity components in x, y, and z directions, respectively. For the pipe, only axial velocity was considered.

$$\begin{aligned}\boldsymbol{u}_T(\boldsymbol{\mu}_k) &= (T_1, ..., T_M)_k^{\mathrm{T}},\\ \boldsymbol{u}_U(\boldsymbol{\mu}_k) &= (U_1, ..., U_M)_k^{\mathrm{T}},\end{aligned} \tag{20}$$

where U denotes axial velocity.

2.2.3 Establishment of reduced-order surrogate model

The surrogate models for each component, including the computational and reconstruction models, are established in this section.

Computational surrogate models were established for reduced-order circuit calculations in which the physical quantity at the outlet of the component was calculated using the inlet variables. As in the previous section, we consider a collection of N output variable snapshots $\boldsymbol{B} = \{\boldsymbol{o}(\boldsymbol{\mu}_k)\}_{k=1}^{N}$. The snapshot for k-th parameter $\boldsymbol{\mu}_k$ is defined as:

$$\boldsymbol{o}(\boldsymbol{\mu}_k) = (T_{\mathrm{out}}, U_{\mathrm{out}}, p_{\mathrm{out}})_k^{\mathrm{T}}, \tag{21}$$

where $T_{\mathrm{out}}, U_{\mathrm{out}}$, and p_{out} are the average outlet temperature, velocity, and pressure, respectively. By establishing a mapping relationship between the inlet and outlet parameters, a computational surrogate model can be established.

$$\boldsymbol{o}(\boldsymbol{\mu}_k) = f(\boldsymbol{\mu}_k) \tag{22}$$

In this study, both linear and RBF interpolation methods were used. A computational model was used for system circuit calculations. This complex system calculation can be simplified by connecting various component computational surrogate models.

After circuit calculation using the computational surrogate model, the reconstruction models were used to reconstruct the one-dimensional or three-dimensional distribution of the kernel physical variables, including the temperature and power distribution of the reactor core and the temperature, velocity, and pressure distribution for SG and pipes. This reconstruction model is based on the mapping relationship between the inlet parameters $\boldsymbol{\mu}$ and basis coefficients c:

$$c_i(\boldsymbol{\mu}_{\mathrm{new}}) = f(\boldsymbol{\mu}_{\mathrm{new}}), \quad i = 1, 2, ..., N_{\mathrm{p}} \tag{23}$$

Subsequently, the variable distribution can be reconstructed as

$$\boldsymbol{u}(\boldsymbol{\mu}_{\mathrm{new}}) = \sum_{i=1}^{N_{\mathrm{p}}} c_i(\boldsymbol{\mu}_{\mathrm{new}})\boldsymbol{P}_i. \tag{24}$$

2.2.4 Multiphysics multiscale circuit reduced-order model

Similar to component surrogate models, the circuit surrogate model is divided into computational and reconstruction models. The computational model connects the inputs and outputs of the computational surrogate models for different components, as shown in Fig. 6. For instance, the output parameters of the reactor core, including the outlet temperature, flow rate, and pressure, served as the input parameters for Heat Section 1. Execution of the circuit ROM computational model begins with the reactor core. Initially, the core power was specified as required and the core inlet parameters were assumed for the calculation. Subsequently, core outlet parameters were determined using a computational surrogate model. Subsequently, the computational surrogate model for each component was executed individually and iterated until the entire circuit model converged. After the ROM computation, the detailed distributions of each component were reconstructed using the reconstruction model, as shown in Fig. 7. For each component, by taking the

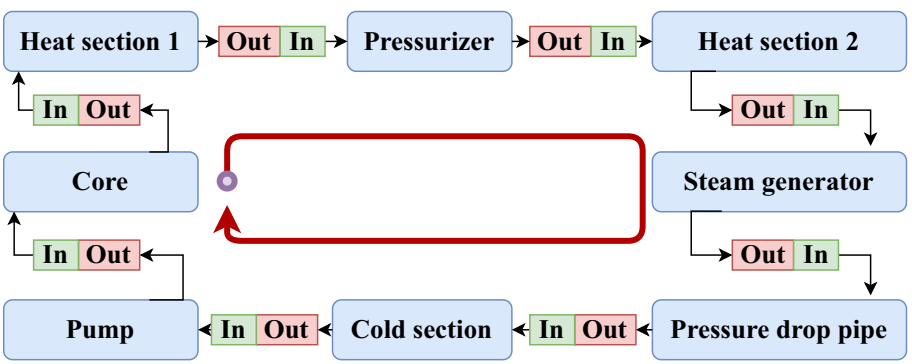

Fig. 6 (Color online) ROM computation model for circuit system

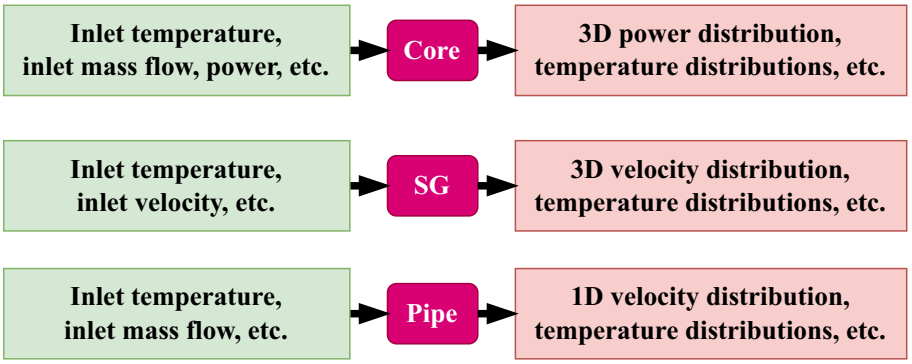

Fig. 7 (Color online) ROM reconstruction model for circuit system

inlet parameters as state parameters to determine the POD coefficients $c_i(\boldsymbol{\mu}_{\text{new}})$, the 1D or 3D distributions can be reconstructed according to Eq. (24).

3 Numerical experiments and result analysis

3.1 Verification of SG CFD model

To verify the accuracy of CFD calculations under void-fraction steam generator conditions, the 100% operating condition of the AP1000 nuclear power plant steam generator was calculated for comparison. Figures 8 and 9 show comparisons between the COMSOL calculation and reference values [69, 70], including the coolant temperature and void fraction. These comparisons show that the COMSOL solutions agree well with the reference values. The design value of the primary-side outlet temperature of the AP1000 nuclear power plant steam generator under 100% steady-state conditions was 553.85 K [71], and the secondary-side outlet mass void fraction based on the cycle ratio design value was approximately 0.27. The calculation results of COMSOL software show that the outlet temperature of the primary side is 554.50 K, and the mass void fraction of the secondary-side outlet is 0.2709, with errors of 0.117% for temperature and 0.333% for void fraction, respectively. These results indicate that the proposed CFD model can be used to simulate the behavior of steam generator under high void-fraction accuracy.

3.2 Snapshots and POD bases

Subsequently, we calculated one-dimensional system models for different core powers and collected the ranges of inlet and outlet parameters, namely, the state parameters (SPs), for different components. For each component, we selected multiple sets of SPs within the ranges listed in Table 1. Subsequently, one-dimensional or three-dimensional multiphysics coupling calculations were performed for each component based on its inlet and outlet state parameter

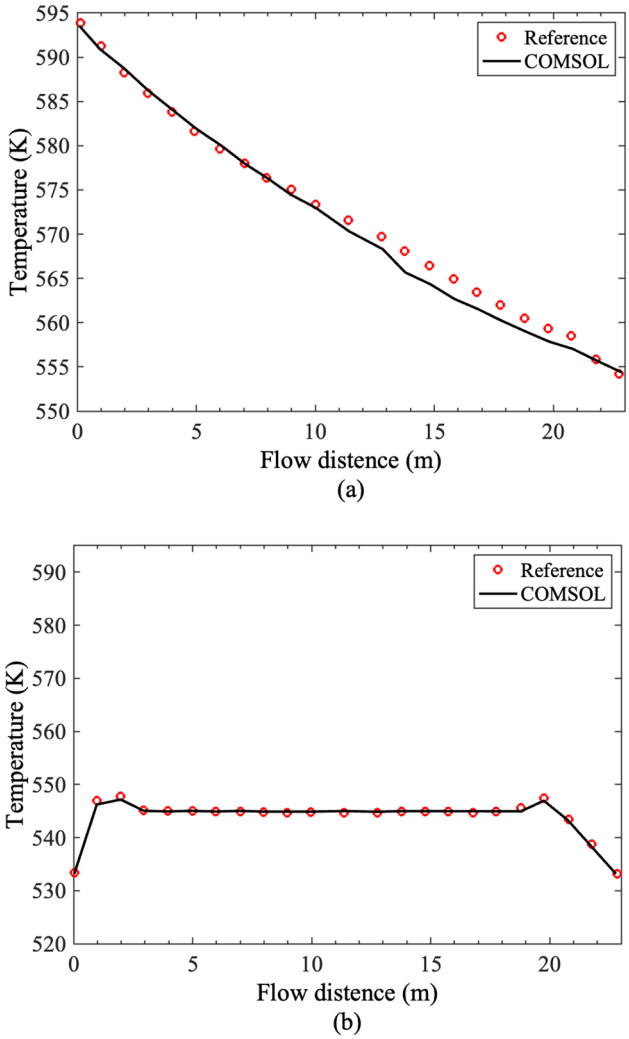

Fig. 8 (Color online) Comparison of steam generation CFD solutions, including (a) primary-side coolant temperature and (b) secondary-side coolant temperature

combinations to obtain component snapshots, including the inlet/outlet parameters and physical quantity distribution within the component.

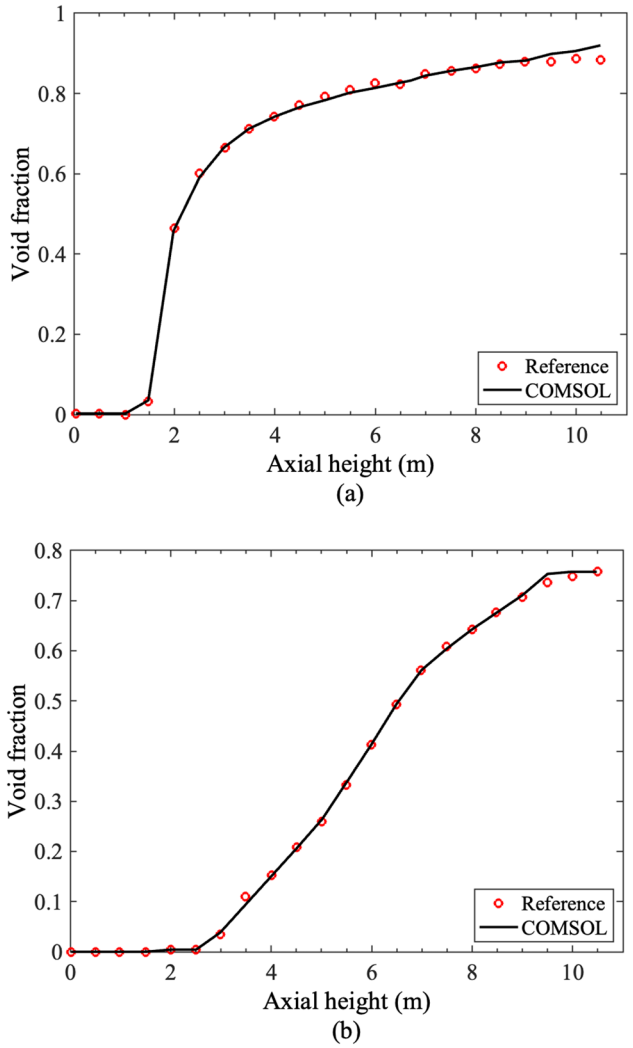

Fig. 9 (Color online) Comparison of steam generation CFD solutions, including (a) cold pipe section void fraction and (b) hot pipe section void fraction

Table 1 State parameters for snapshot calculations

Component	SPs	Values	No. state points
Core	G_{in}	79.9, 80.9, ..., 96.9	17
	T_{in}	279, 279.5, ..., 283	9
	p_{in}	15.3, 15.4, ..., 16	8
SG	U_{in}	5.5, 5.55, 5.6	3
	T_{in}	291, 293.5, ..., 331	17
	p_{out}	15.45, 15.5	2
Heat pipe	U_{in}	13, 13.5,...,15.5	5
	T_{in}	290, 295, ..., 330	9
	p_{in}	15,15.5,16	3
Pressure pipe	U_{in}	18,18.5,19,19.5	4
	T_{in}	280, 282.5, ..., 285	3
	p_{in}	15.4,15.5,15.6	3
Cold section	U_{in}	25,25.5,26	3
	T_{in}	280, 282.5, ..., 285	3
	p_{in}	15.4,15.5,...,16	7

Table 2 POD order for each component

Component	Variable	POD order
Core	P	5
	T	4
SG	T	16
	u	4
	v	46
	w	22
Heat pipe	T	1
	U	2
Pressure pipe	T	1
	U	2
Cold section	T	1
	U	2

The POD bases of each component were calculated from these snapshots and the main POD orders for each component were determined using Eq. (17) as listed in Table 2. The distributions in the reactor core and pipes can be predicted using lower-order POD bases, whereas the temperature and velocity distributions of the steam generator require relatively high POD orders. This is because the fluid flow within SG is simulated using the 3D CFD method, which captures the extremely complex flow characteristics inside SG and therefore requires higher POD orders. In the steam generator, u is mainly concentrated in the curved sections with slight variations, which can be reconstructed using a small number of POD bases. v is the velocity component along the radial direction, with relatively small values but noticeable fluctuations throughout the pipe, thus requiring a larger number of POD bases. w is primarily concentrated in the straight sections of the pipe and exhibits significant variations in the curved section. Thus, it also requires a larger number of POD bases.

Figures 10 and 11 show the first five POD bases of the power and four POD bases of the temperature distributions. These images show that the first-order power basis characterizes the overall power distribution characteristics of the core, whereas the higher-order bases characterize the power characteristics of different core regions, including the CR insertion and absence regions. The first-order temperature basis characterized the overall temperature distribution of the core. The second- and fourth-order bases characterized the temperature characteristics of the reflector and active regions, whereas the third basis

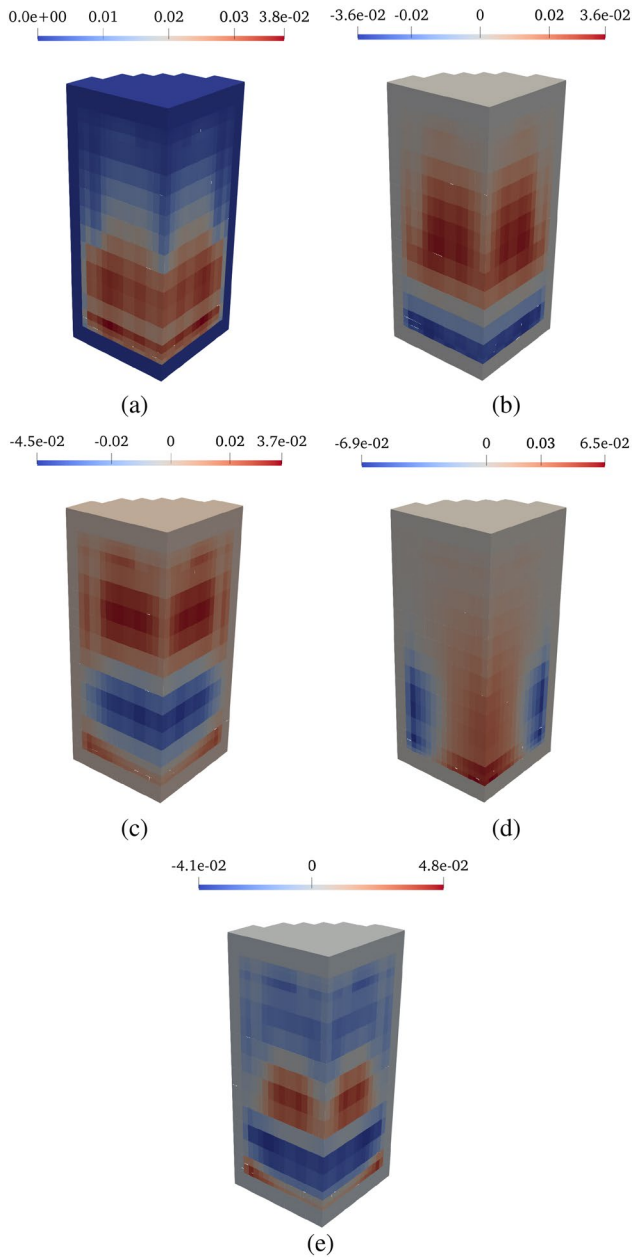

Fig. 10 (Color online) First five POD bases of core power (kW/cm^3), including (a) the first-order power basis, (b) the second-order power basis, (c) the third-order power basis, (d) the fourth-order power basis, and (e) the fifth-order power basis

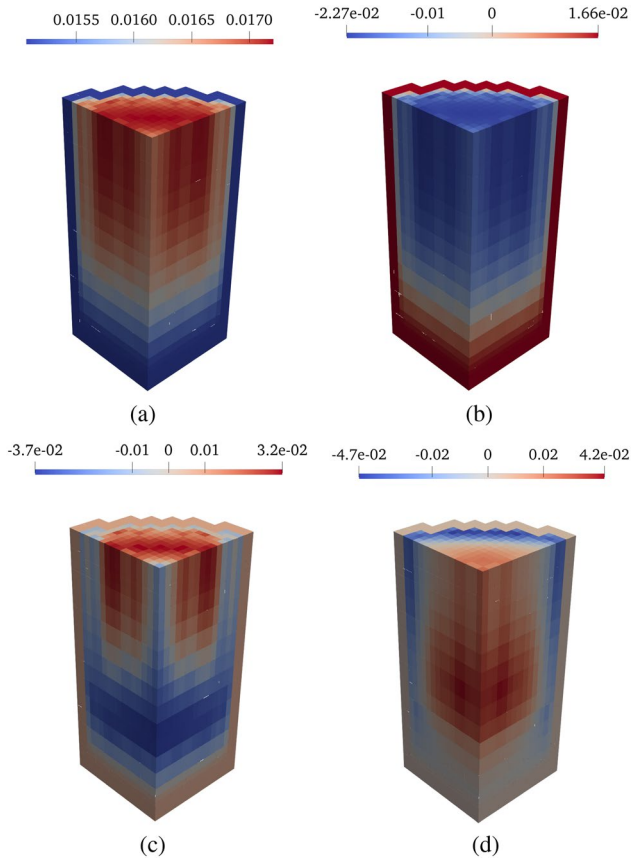

Fig. 11 (Color online) First four POD bases of core temperature (°C), including (a) the first-order temperature basis, (b) the second-order temperature basis, (c) the third-order temperature basis, and (d) the fourth-order temperature basis

characterized the temperature characteristics of the core outlet.

3.3 Results and discussions

After obtaining the POD bases of each component, we built a reduced-order surrogate model for each component and connected all the surrogate models to form a reduced-order primary circuit system. Figure 12 shows the 1D temperature and velocity distributions along the length of the primary circuit system, the FOM and ROM solutions are compared with each other. In addition, the relative errors of the ROM calculation for 1D temperature and velocity distributions were less than 0.04%, indicating that the proposed digital twin based on the ROM can be used to predict the primary circuit system accurately. Only the inlet and outlet variables of the reactor core and steam generator are included in this figure, and their detailed distribution will be analyzed later.

To further analyze the accuracy of the proposed digital twin in multiscale multiphysics prediction, the 3D distributions within the reactor core and steam generator were compared with the FOM results. Figures 13 and 14 show the core power and temperature distributions predicted by the ROM, respectively, and the relative errors between the ROM and FOM results are compared. The maximum temperature and power errors of the reactor core were 0.0207% and 0.0252%, respectively, indicating the high accuracy of the proposed ROM surrogate for 3D reactor core multiphysics prediction. Furthermore, the key thermal-hydraulic parameters of the nuclear reactor, including the average fuel temperature

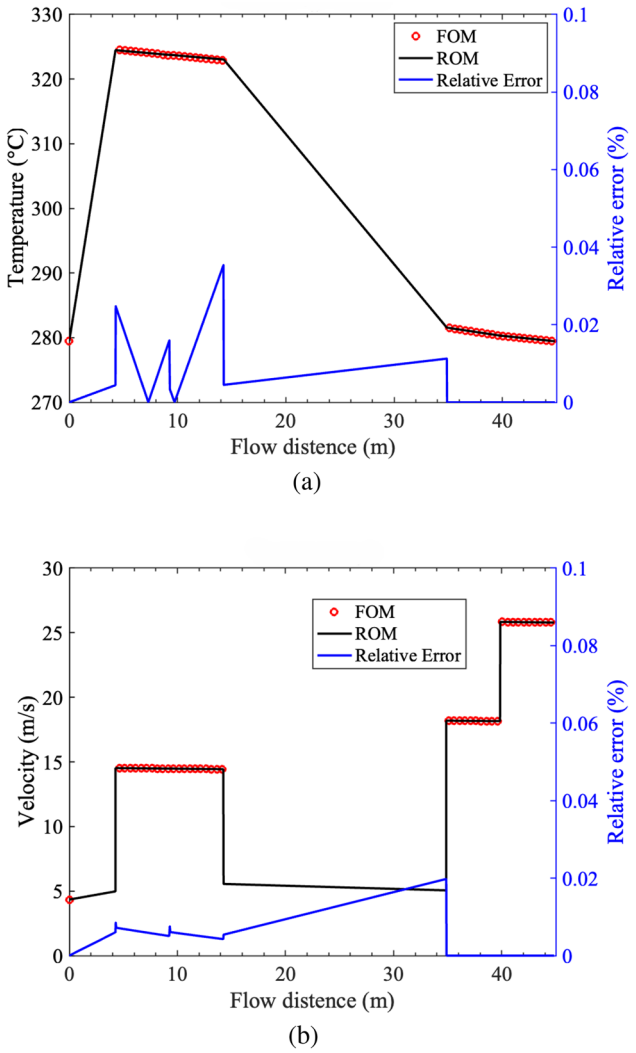

Fig. 12 (Color online) Comparison of variable distributions for the primary circuit, including (a) temperature distribution and (b) velocity distribution

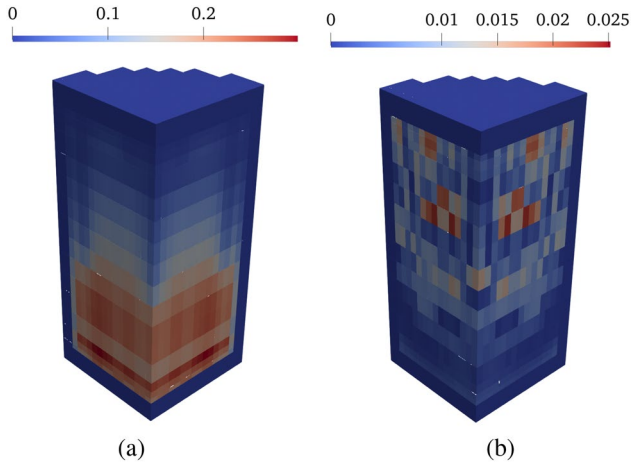

Fig. 13 (Color online) Solution of the ROM core power prediction, including (a) ROM power distribution (kW/cm^3), and (b) relative error between ROM and FOM (%)

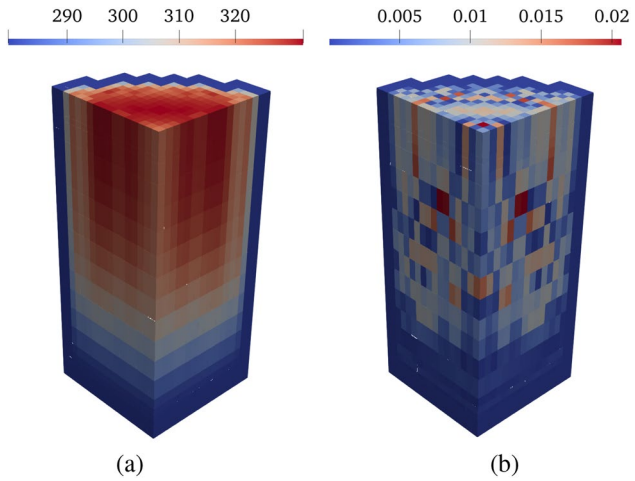

Fig. 14 (Color online) Solution of the ROM core temperature prediction, including (a) ROM temperature distribution (°C), and (b) relative error between ROM and FOM (%)

$T_{u,ave}$, maximum fuel centerline temperature $T_{u,max}$, average moderator temperature $T_{m,ave}$, and maximum moderator temperature $T_{m,max}$ are compared, as shown in Table 3. All these variables show a high accuracy of ROM prediction, with a maximum error of 0.018%.

Subsequently, the predictions of the 3D steam generator are compared. Figure 15 shows the axial temperature distribution along the pipeline direction, and Fig. 16 shows the typical temperature distributions at different cross sections. These images show that the heat on the primary side was gradually removed by the secondary fluid during the flow process, resulting in a gradual decrease in the temperature of the coolant on the primary side. The ROM solution shows good agreement with that of the FOM calculation, and the maximum relative error is no larger than 0.05%, indicating

Table 3 Comparison of typical reactor parameters

	FOM	ROM	Relative error (%)
$T_{u,ave}$ (°C)	601.55	601.53	3.32×10^{-3}
$T_{u,max}$ (°C)	2118.25	2118.25	0
$T_{m,ave}$ (°C)	308.95	308.96	3.24×10^{-3}
$T_{m,max}$ (°C)	331.85	331.91	0.018

that the proposed SG surrogate of the steam generator can be used to predicate the 3D detailed distribution accurately.

The ROM calculation time was only 0.0017 s, whereas that of the full-order model was several hours. This indicated

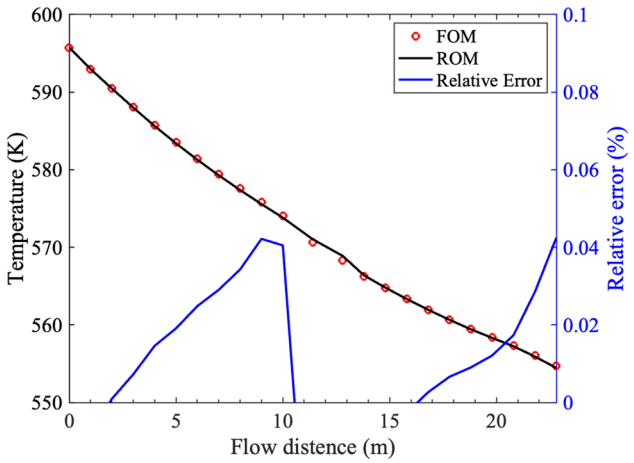

Fig. 15 (Color online) Comparison of the axial temperature of the steam generator

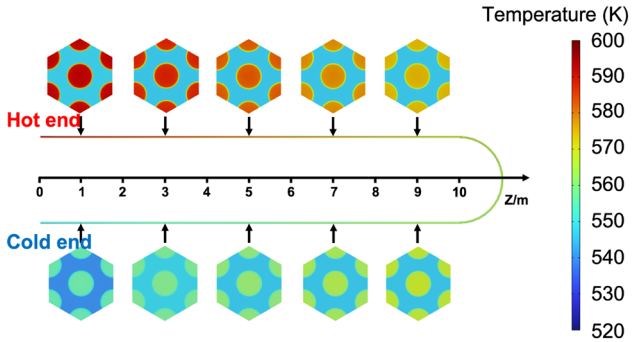

Fig. 16 (Color online) Temperature distribution of steam generator at different cross sections

that the ROM calculation was significantly faster than the FOM calculation.

The reduced-order model can be used to predict the multiscale multiphysics behavior of a primary circuit system with high accuracy and high calculation speed.

4 Conclusions and prospect

In this study, a plug-and-play digital twin based on a multiscale multiphysics reduced-order model for nuclear reactor system circuits was established. Surrogate models for the key components were constructed using a three-dimensional model, and surrogate models for the other devices were constructed using a one-dimensional model, effectively reducing the computational cost of snapshots. According to the design and analysis requirements of nuclear reactor systems, surrogate models of the corresponding components can be selected, and digital twin circuits can be constructed plug-and-play by connecting these surrogate models. A complicated multiscale and multiphysics simulation of the reactor circuit can be easily achieved using these surrogate models. The accuracy and efficiency of the proposed reduced-order model are verified by comparing the results with those of a full-order model in a typical system circuit. Good agreement between the ROM and FOM was obtained, including the 1D and detailed 3D solutions. The maximum relative error of the ROM was $< 0.05\%$. The computing time of the digital twin circuit is less than 2 ms, which is much lower than the FOM computing time, and has the potential to achieve real-time or even ultra-real-time system circuit prediction.

The work presented in this paper is the first step toward the digital twin of nuclear reactor systems, focusing on the multiscale, multiphysics, and steady-state behavior of nuclear reactor circuit systems under normal operating conditions. Further research is required to advance this field, particularly in the following areas.

1. To broaden the applicability of the current study, a more comprehensive library of component surrogate models will be developed for a wider range of nuclear power systems, such as Gen-IV commercial reactors and small modular reactors.
2. To enable the prediction of system behavior during accident and power change operations, transient prediction surrogate models for system components, as well as a transient digital twin loop, need to be established.
3. To analyze the system behavior under complex conditions, detailed surrogate models for additional components, such as pressurizers, main pumps, and valves, will be developed. Additionally, more refined simulation methods, such as pin-by-pin neutronics calculations and subchannel thermal-hydraulic analyses, will be applied to the reactor core for snapshots.
4. Finally, to apply the proposed method to nuclear reactor engineering, tests and verification based on realistic measurement data from nuclear power plants must be conducted.

Author contributions All authors contributed to the study conception and design. Material preparation, data collection and analysis were performed by Ya-Hui Wang, Ze-Long Zhao, Zhe-Xian Liu, Hong-Hang Chi and Yu Ma. The first draft of the manuscript was written by Ya-Hui Wang, and all authors commented on previous versions of the manuscript. All authors read and approved the final manuscript.

Data availability The data that support the findings of this study are openly available in Science Data Bank at https://cstr.cn/31253.11.sciencedb.j00186.00949 and https://www.doi.org/10.57760/sciencedb.j00186.00949.

Declarations

Conflict of interest The authors declare that they have no conflict of interest.

References

1. K.M. Yassin, M.H. Hassan, M.M. Ghoneim et al., Multiphysics simulation of VVER-1200 fuel performance during normal operating conditions. Nucl. Sci. Tech. **34**, 28 (2023). https://doi.org/10.1007/s41365-023-01172-9
2. C.L. Wang, T.C. Liu, S.M. Tang et al., Thermal-hydraulic analysis of space nuclear reactor TOPAZ-II with modified RELAP5. Nucl. Sci. Tech. **30**, 12 (2019). https://doi.org/10.1007/s41365-018-0537-3
3. M.S. Sena, Y.A. Hassan, Thermal-hydraulic behavior simulations of the reactor cavity cooling system (RCCS) experimental facility using Flownex. Nucl. Eng. Technol. **55**(9), 3320–3325 (2023). https://doi.org/10.1016/j.net.2023.05.023
4. C.B. Shi, M.S. Chen, G.M. Liu, Development and application of a system analysis code for liquid fueled molten salt reactors based on RELAP5 code. Nucl. Eng. Des. **305**(15), 378–388 (2016). https://doi.org/10.1016/j.nucengdes.2016.05.034
5. Z.X. Gu, Q.X. Zhang, Y. Gu et al., Verification of a self-developed CFD-based multi-physics coupled code MPC-LBE for LBE-cooled reactor. Nucl. Sci. Tech. **32**, 52 (2021). https://doi.org/10.1007/s41365-021-00887-x
6. M. Wang, Y. Wang, W. Tian et al., Recent progress of CFD applications in PWR thermal hydraulics study and future directions. Ann. Nucl. Energ. **150**, 107836 (2021). https://doi.org/10.1016/j.anucene.2020.107836
7. X. Luo, C. Wang, Z.R. Zou et al., Development and application of a multi-physics and multi-scale coupling program for lead-cooled fast reactor. Nucl. Sci. Tech. **33**, 18 (2022). https://doi.org/10.1007/s41365-022-01008-y
8. H.R. Qiu, M.J. Wang, J. Zhang et al., Multi-scale coupling analysis of the flow blockage accident in the typical LFR. Int. J. Therm. Sci. **195**, 108615 (2024). https://doi.org/10.1016/j.ijthermalsci.2023.108615
9. A.G. Mylonakis, M. Varvayanni, N. Catsaros et al., Multi-physics and multi-scale methods used in nuclear reactor analysis. Ann. Nucl. Energ. **72**, 104–119 (2014). https://doi.org/10.1016/j.anucene.2014.05.002
10. L. Wei, L.M. Pan, H. He et al., Numerical study on single-phase flow of natural circulation under ocean condition using coupled relap5 system code and fluent code. Nucl. Eng. Des. **343**, 138–150 (2019). https://doi.org/10.1016/j.nucengdes.2019.01.003
11. P.J. Turinsky, D.B. Kothe, Modeling and simulation challenges pursued by the Consortium for Advanced Simulation of Light Water Reactors (CASL). J. Comput. Phys. **313**, 367–376 (2016). https://doi.org/10.1016/j.jcp.2016.02.043
12. B. Chanaron, C. Ahnert, N. Crouze et al., Advanced multi-physics simulation for reactor safety in the framework of the NURESAFE project. Ann. Nucl. Energ. **84**, 166–177 (2015). https://doi.org/10.1016/j.anucene.2014.12.013
13. T.P. Grunloh, A. Manera, A novel multi-scale domain overlapping CFD/STH coupling methodology for multi-dimensional flows relevant to nuclear applications. Nucl. Eng. Des. **318**, 85–108 (2017). https://doi.org/10.1016/j.nucengdes.2017.03.027
14. W.H. Cai, Z.M. Li, J. Cui et al., A new multi-scale coupling simulation of natural circulation system based on self-adaption data interaction method. Ann. Nucl. Energ. **186**, 109758 (2023). https://doi.org/10.1016/j.anucene.2023.109758
15. J.Y. Cao, J.C. Sun, X.F. Meng et al., Study on multi-scale coupled simulation of natural circulation system with 3 × 3 petal-shaped fuel bundle channel under rolling condition. Ann. Nucl. Energ. **198**, 110332 (2024). https://doi.org/10.1016/j.anucene.2023.110332
16. A. Papukchiev, G. Lerchl, C. Waata et al., Extension of the simulation capabilities of the 1D system code ATHLET by coupling with the 3D CFD software package ANSYS CFX. Proceedings of the 13th international topical meeting on nuclear reactor thermal-hydraulics (NURETH-13), Kanazawa, Japan, 2009
17. R. Baviere, N. Tauveron, F. Perdu et al., A first system/CFD coupled simulation of a complete nuclear reactor transient using CATHARE2 and TRIO_U Preliminary validation on the Phénix reactor natural circulation test. Nucl. Eng. Des. **277**, 124–137 (2014). https://doi.org/10.1016/j.nucengdes.2014.05.031
18. Z.R. Zou, C. Shen, X.L. Zhang et al., 3D thermal hydraulic characteristics analysis of pool-type upper plenum for lead-cooled fast reactor with multi-scale coupling program. Nucl. Eng. Des. **370**, 110892 (2020). https://doi.org/10.1016/j.nucengdes.2020.110892
19. W. Zhao, L.X. Chen, G.D. Liu et al., Study on multi-scale thermal-hydraulic coupling strategy under the steady state of Xi'an pulsed reactor. Ann. Nucl. Energ. **182**, 109586 (2023). https://doi.org/10.1016/j.anucene.2022.109586
20. V.H. Sanchez-Espinoza, K. Zhang, M.A. Campos et al., KIT Multi-scale thermal–hydraulic coupling methods for improved simulation of nuclear power plants. Nucl. Eng. Des. **405**, 112218 (2023). https://doi.org/10.1016/j.nucengdes.2023.112218
21. I.K. Park, J.R. Lee, Y.H. Choi et al., A multi-scale and multi-physics approach to main steam line break accidents using coupled MASTER/CUPID/MARS code. Ann. Nucl. Energ. **135**, 106972 (2020). https://doi.org/10.1016/j.anucene.2019.106972
22. J.R. Lee, H.Y. Yoon, J.Y. Park, Transient full core analysis of PWR with multi-scale and multi-physics approach. Nucl. Eng. Technol. **56**, 980–992 (2024). https://doi.org/10.1016/j.net.2023.12.006
23. S. Gallardo, F. Alvarez-Velarde, T. Barrachina et al., Development and application in multiscale and multiphysics methodologies in Spain: Present and future trends. Nucl. Eng. Des. **421**, 113096 (2024). https://doi.org/10.1016/j.nucengdes.2024.113096
24. D.E. Keyes, L.C. McInnes, C. Woodward et al., Multiphysics simulations: Challenges and opportunities. Int. J. High Perform. C. **27**(1), 4–83 (2013). https://doi.org/10.1177/1094342012468181
25. H.L. Gong, S.B. Cheng, Z. Chen et al., An efficient digital twin based on machine learning SVD autoencoder and generalised latent assimilation for nuclear reactor physics. Ann. Nucl. Energ. **179**, 109431 (2022). https://doi.org/10.1016/j.anucene.2022.109431
26. H.L. Gong, H. Li, D.H. Xiao et al., Reactor field reconstruction from sparse and movable sensors using Voronoi tessellation-assisted convolutional neural networks. Nucl. Sci. Tech. **35**, 43 (2024). https://doi.org/10.1007/s41365-024-01400-w
27. Q.H. Yang, Y. Yang, Y.T. Deng et al., Physics-Constrained neural network for solving discontinuous interface K-eigenvalue problem with application to reactor physics. Nucl. Sci. Tech. **34**, 161 (2023). https://doi.org/10.1007/s41365-023-01313-0
28. B.A. Khuwaileh, P.J. Turinsky, Surrogate based model calibration for pressurized water reactor physics calculations. Nucl. Eng. Technol. **49**(6), 1219–1225 (2017). https://doi.org/10.1016/j.net.2017.08.007
29. A. Marrel, N. Marie, M. De Lozzo, Advanced surrogate model and sensitivity analysis methods for sodium fast reactor accident assessment. Reliab. Eng. Syst. Saf. **138**, 232–241 (2015). https://doi.org/10.1016/j.ress.2015.01.019
30. H.L. Gong, S.B. Cheng, Z. Chen et al., Data-enabled physics-informed machine learning for reduced-order modeling digital twin: application to nuclear reactor physics. Nucl. Sci. Eng.

196(6), 668–693 (2022). https://doi.org/10.1080/00295639.2021.2014752
31. M.W. Guo, J.S. Hesthaven, Data-driven reduced order modeling for time-dependent problems. Comput. Methods Appl. Mech. Energ. **345**, 75–99 (2019). https://doi.org/10.1016/j.cma.2018.10.029
32. S. Dutta, M.W. Farthing, E. Perracchione et al., A greedy non-intrusive reduced order model for shallow water equations. J. Comp. Phys. **439**, 110378 (2021). https://doi.org/10.1016/j.jcp.2021.110378
33. J. Yu, C. Yan, M.W. Guo, Non-intrusive reduced-order modeling for fluid problems: A brief review. Proceedings of the Institution of Mechanical Engineers, Part G: Journal of Aerospace Engineering **233**, 5896–5912 (2019). https://doi.org/10.1177/0954410019890721
34. M.I. Younis, E.M. Abdel-Rahman, A. Nayfeh, A reduced-order model for electrically actuated microbeam-based MEMS. J. Microelectromech. S. **12**, 672–680 (2003). https://doi.org/10.1109/JMEMS.2003.818069
35. Y.S. Cai, S. van Ophem, W. Desmet et al., Model order reduction of time-domain vibro-acoustic finite element simulations with non-locally reacting absorbers. Comput. Methods Appl. Mech. Energ. **416**, 116345 (2023). https://doi.org/10.1016/j.cma.2023.116345
36. V. Mehtab, S. Alam, S. Povari et al., Reduced order machine learning models for accurate prediction of CO_2 capture in physical solvents. Environ. Sci. Technol. **57**, 18091–18103 (2023). https://doi.org/10.1021/acs.est.3c00372
37. F. Alsayyari, M. Tiberga, Z. Perkó et al., Analysis of the Molten Salt Fast Reactor using reduced-order models. Prog. Nucl. Energ. **140**, 103909 (2021). https://doi.org/10.1016/j.pnucene.2021.103909
38. H.L. Gong, Y.R. Yu, X.J. Peng et al., A data-driven strategy for xenon dynamical forecasting using dynamic mode decomposition. Ann. Nucl. Energ. **149**, 107826 (2020). https://doi.org/10.1016/j.anucene.2020.107826
39. K.A. Dominesey, W. Ji, Reduced-order modeling of neutron transport eigenvalue problems separated in energy by Proper Generalized Decomposition. J. Comp. Phys. **486**, 112137 (2023). https://doi.org/10.1016/j.jcp.2023.112137
40. C.E. Heaney, A.G. Buchan, C.C. Pain et al., Reduced-order modelling applied to the multigroup neutron diffusion equation using a nonlinear interpolation method for control-rod movement. Energies **14**, 1350 (2021). https://doi.org/10.3390/en14051350
41. P. German, J.C. Ragusa, Reduced-order modeling of parameterized multi-group diffusion k-eigenvalue problems. Ann. Nucl. Energ. **134**, 144–157 (2019). https://doi.org/10.1016/j.anucene.2019.05.049
42. J.A. Roberts, L. Xu, R. Elzohery et al., Acceleration of the power method with dynamic mode decomposition. Nucl. Sci. Eng. **193**(12), 1371–1378 (2019). https://doi.org/10.1080/00295639.2019.1634928
43. W. Chen, D. Yang, J.J. Zhang et al., Study of non-intrusive model order reduction of neutron transport problems. Ann. Nucl. Energ. **162**, 108495 (2021). https://doi.org/10.1016/j.anucene.2021.108495
44. H.H. Chi, Y.H. Wang, Y. Ma, Reduced-order with least square-finite difference method for neutron transport equation. Ann. Nucl. Energ. **191**, 109914 (2023). https://doi.org/10.1016/j.anucene.2023.109914
45. Y.H. Wang, H.H. Chi, Y. Ma, Nodal expansion method based reduced-order model for control rod movement. Ann. Nucl. Energ. **198**, 110279 (2024). https://doi.org/10.1016/j.anucene.2023.110279
46. H.H. Chi, Y. Ma, Y.H. Wang, Reduced-order methods for neutron transport kinetics problem based on proper orthogonal decomposition and dynamic mode decomposition. Ann. Nucl. Energ. **206**, 110641 (2024). https://doi.org/10.1016/j.anucene.2024.110641
47. J.P. Argaud, B. Bouriquet, F. de Caso et al., Sensor placement in nuclear reactors based on the generalized empirical interpolation method. J. Comp. Phys. **363**, 354–370 (2018). https://doi.org/10.1016/j.jcp.2018.02.050
48. F. Alsayyari, M. Tiberga, Z. Perkó et al., Analysis of the Molten Salt Fast Reactor using reduced-order models. Prog. Nucl. Energ. **140**, 103909 (2021). https://doi.org/10.1016/j.pnucene.2021.103909
49. P. German, M. Tano, C. Fiorina et al., GeN-ROM—An OpenFOAM®-based multiphysics reduced-order modeling framework for the analysis of Molten Salt Reactors. Prog. Nucl. Energ. **146**, 104148 (2022). https://doi.org/10.1016/j.pnucene.2022.104148
50. H. Kang, Z. Tian, G. Chen et al., Application of POD reduced-order algorithm on data-driven modeling of rod bundle. Nucl. Eng. Tech. **54**, 36–48 (2022). https://doi.org/10.1016/j.net.2021.07.010
51. V. Lorenzo, C. Antonio, L. Stefano, Reduced order modeling for coupled thermal-hydraulics and reactor physics problems. Prog. Nucl. Eng. **140**, 103899 (2022). https://doi.org/10.1016/j.pnucene.2021.103899
52. S.K. Star, G. Spina, F. Belloni et al., Development of a coupling between a system thermal-hydraulic code and a reduced order CFD model. Ann. Nucl. Energ. **153**, 108056 (2021). https://doi.org/10.1016/j.anucene.2020.108056
53. R. Manther, A. Knospe, C. Lange et al., Reduced order modeling of a natural circulation system by proper orthogonal decomposition. Prog. Nucl. Energ. **114**, 191–200 (2019). https://doi.org/10.1016/j.pnucene.2019.03.010
54. X.G. Chen, H.R. Wang, H. Zhang et al., A digital twin model of the axial temperature field of a DC cable for millisecond calculations. Electr. Pow. Syst. Res. **233**, 110460 (2024). https://doi.org/10.1016/j.epsr.2024.110460
55. J. Zheng, D.Z. Jiang, X. Jia et al., A new meshless approach for marine power component modelling using digital twin reduced-order technique. Eng. Anal. Bound. Elem. **153**, 242–250 (2023). https://doi.org/10.1016/j.enganabound.2023.05.027
56. R.D. Lawrence, Progress in nodal methods for the solution of the neutron diffusion and transport equations. Prog. Nucl. Energ. **17**(3), 271–301 (1986). https://doi.org/10.1016/0149-1970(86)90034-X
57. K. Sadeghi, S.H. Ghazaie, E. Sokolova et al., A set of transient correlations for fast and unprotected loss of flow accident in VVER-1000 reactor using single-heated channel approach and Gene Expression Programming. Ann. Nucl. Energ. **183**, 109650 (2023). https://doi.org/10.1016/j.anucene.2022.109650
58. H. Mohammad, K. Hossein, K. Samad, Two group, three dimensional diffusion theory coupled with single heated channel model: A study based on xenon transient simulation of Tehran research reactor. Prog. Nucl. Energ. **85**, 108–120 (2015). https://doi.org/10.1016/j.pnucene.2015.06.009
59. J.R. Cooper, R.B. Dooley, The international association for the properties of water and steam (revised release on the IAPWS industrial formulation 1997 for the thermodynamic properties of water and steam), IAPWS R7–97 (2007)
60. M. Imron, Development and verification of open reactor simulator ADPRES. Ann. Nucl. Energ. **133**, 580–588 (2019). https://doi.org/10.1016/j.anucene.2019.06.049
61. Y.J. Li, Y.L. Yang, B.Z. Sun, Numerical investigation of thermal–hydraulic characteristics in a steam generator using a coupled primary and secondary side heat transfer model. Ann. Nucl. Energ. **55**, 258–264 (2013). https://doi.org/10.1016/j.anucene.2012.11.025

62. B.Z. Sun, Y.L. Yang, Numerically investigating the influence of tube support plates on thermal hydraulic characteristics in a steam generator. Appl. Therm. Eng. **51**, 611–622 (2013). https://doi.org/10.1016/j.applthermaleng.2012.10.009
63. ANSYS-Inc, ANSYS CFX 18.0: Users Manual, 2017
64. R.W. Pryor, Multiphysics modeling using COMSOL: a first principles approach. Jones & Bartlett Publishers, 2009
65. A. Dehbi, H. Badreddine, CFD prediction of mixing in a steam generator mock-up: Comparison between full geometry and porous medium approaches. Ann. Nucl. Energ. **58**, 178–187 (2013). https://doi.org/10.1016/j.anucene.2013.03.019
66. I.E. Idelchik. Handbook of hydraulic resistance, United States (1986)
67. B. Sutharshan, M. Mutyala, R.P. Vijuk et al., The AP1000^{TM} reactor: passive safety and modular design. Energy Proced. **7**, 293–302 (2011). https://doi.org/10.1016/j.egypro.2011.06.038
68. R.S. Zhu, Y. Liu, X.L. Wang et al., The research on AP1000 nuclear main pumps' complete characteristics and the normalization method. Ann. Nucl. Energ. **99**, 1–8 (2017). https://doi.org/10.1016/j.anucene.2016.08.014
69. Z.G. Sui, J. Yang, X.Y. Zhang et al., Numerical investigation of the thermal-hydraulic characteristics of AP1000 steam generator U-tubes. Int. J. Adv. Nucl. Reac. Des. Technol. **2**, 52–59 (2020). https://doi.org/10.1016/j.jandt.2020.09.001
70. Z.G. Sui, Numerical investigation of the thermal-hydraulic characteristics of PWR steam generator based on CFD. Huazhong University of Science and Technology, 2020
71. Westinghouse, AP1000 design control document revison 19. Pittsburg: Westinghouse Electric Corporation, 2011